Appendix A

Regge pole phenomenology

A.1 Regge pole

Aside from the theory of quarks and gluons, there have been an old phenomenological approach to explain the asymptotic behavior of the hadron-hadron collisions. This phenomenology is called *Regge pole phenomenology* or Regge theory in short. In the framework of the Regge theory, a soft hadron-hadron collision is described by the exchange of bunch of mesons which have adequate quantum numbers for the exchange process. Those exchanged objects are called *Regge poles.*

Outline of the Regge theory is briefly described here using 2→2 scattering of spin less particles [2, 3]. The Mandelstem variables s and t are used. The s is a center of mass energy squared and the t is a momentum transfer squared. The Lorentz invariant amplitude of the 2→2 scattering process can be expressed by the partial wave expansion,

$$A_{a\bar{c}\to\bar{b}d}(s,t) = \sum_{l=0}^{\infty}(2l+1)a_l(s)P_l(1+2t/s), \tag{A.1}$$

where l is a quantum number of orbital angular momentum and P_l is a Legendre polynomial. This expression can be transformed into the following form using the crossing symmetry,

$$A_{ab\to cd}(s,t) = \sum_{l=0}^{\infty}(2l+1)a_l(t)P_l(1+2s/t). \tag{A.2}$$

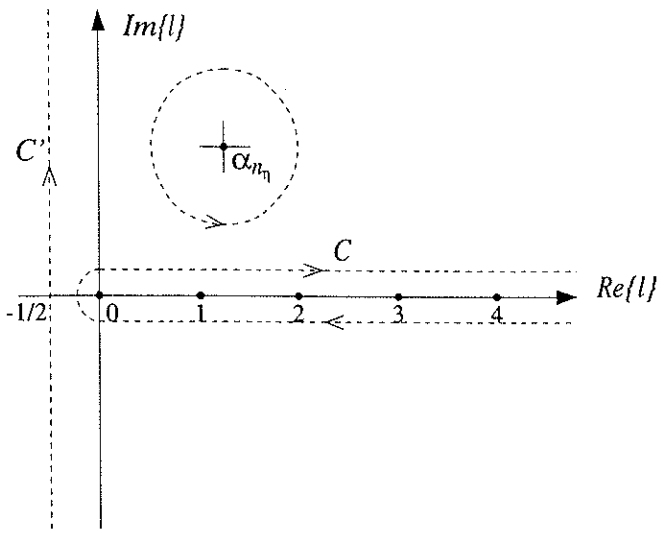

Figure A.1: Complex angular momentum plane.

The summation about l can be rewritten into the integral form in the complex angular momentum plane using the analytic property of the amplitude,

$$A(s,t) = \frac{1}{2i}\oint_C dl\,\frac{(2l+1)}{\sin\pi l}\sum_{\eta=\pm1}\frac{\left(\eta+e^{-i\pi l}\right)}{2}a^{(\eta)}(l,t)P(l,1+2t/s), \qquad \text{(A.3)}$$

where the contour C surrounds the positive real axis as shown in Fig. A.1. $a^{(+1)}$ and $a^{(-1)}$ are the analytic continuations of the even and odd partial wave amplitude. The η takes the values ±1 and is called the signature of the partial wave. The signature is introduced to separate two alternating signed amplitudes owing to the term of $(-1)^l$. Let us suppose for simplicity that the system has just isolated poles at $l{=}\alpha_{n_\eta}(t)$ of the form $a^{(\eta)}(l,t){=}\beta_{n_\eta}(t)(l-\alpha_{n_\eta}(t))^{-1}$. The above integral can be reduced into the sum of the residuals by deforming the contour C into the contour C' as shown in Fig. A.1. For this particular case we arrive at

$$A(s,t) = \sum_{\eta=\pm1}\sum_{n_\eta}\frac{\left(2\alpha_{n_\eta}(t)+1\right)}{\sin\pi\alpha_{n_\eta}(t)}\frac{\left(\eta+e^{-i\pi\alpha_{n_\eta}(t)}\right)}{2}\beta_{n_\eta}(t)P\left(\alpha_{n_\eta}(t),1+2s/t\right) + (\text{integral on } C'). \qquad \text{(A.4)}$$

The simple poles $\alpha_{n_\eta}(t)$ are called *Regge poles*. When we take a limit of $s/|t|\to\infty$, the integral term along the contour C' behaves as $\sim s^{-1/2}$ and so

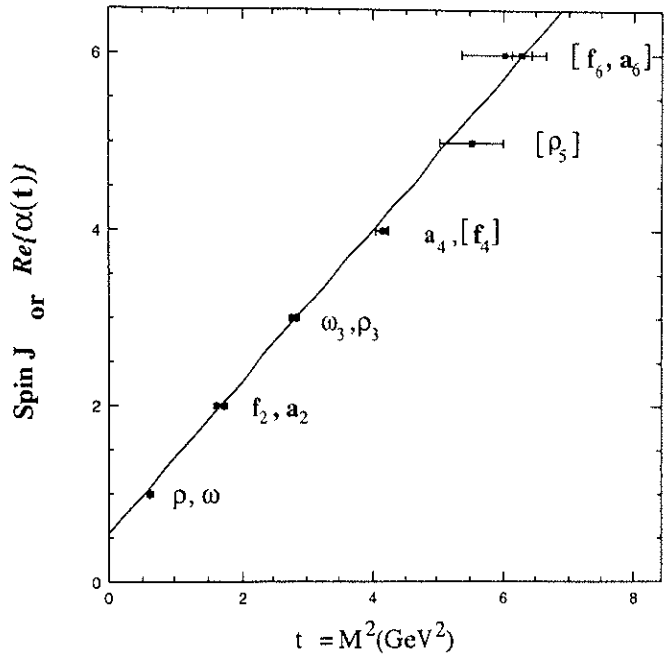

Figure A.2: The Chew-Frautschi plot.

it vanishes. In general, the existence of a single particle state in a theory is appeared as a pole in the transition amplitude. Thus Eq.A.4 shows that the Regge pole with a physical integer value of $l = \Re\mathrm{e}\{\alpha_{n_\eta}(t)\}$ corresponds to a particle with spin-l. In this picture, the scattering process can be interpreted as exchange of the Regge pole (or *Reggeon*) with adequate quantum numbers in the exchange process.

In the high energy limit, the dominant term among the residuals in Eq.A.4 comes from the Regge pole with the largest value of $\Re\mathrm{e}\{\alpha_{n_\eta}(t)\}$ (leading Regge trajectory). Eq.A.4 can be then approximated to,

$$A(s,t) \sim s^{\alpha(t)}, \tag{A.5}$$

where we used asymptotic behavior of the Legendre polynomial,

$$P_l\left(1+2s/t\right) \xrightarrow{s\gg|t|} \frac{\Gamma(2l+1)}{\Gamma^2(l+1)}\left(\frac{s}{t}\right)^l.$$

The function shape of the $\Re\mathrm{e}\{\alpha(t)\}$ can be investigated by plotting the spin against the square of the mass for existing particles. Figure A.2 shows the

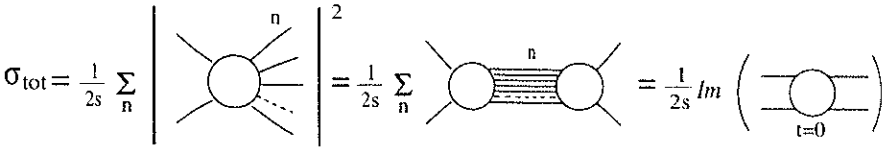

Figure A.3: Optical theorem.

mesons which can be exchanged in the $p\bar{p} \to p\bar{p}$ scattering process. Those mesons lie in a straight line as shown in the plot and this property means the trajectory of the $\alpha(t)$ is a linear function of t,

$$\alpha(t) = \alpha(0) + \alpha' t$$

where

$$\alpha(0) = 0.55$$
$$\alpha' = 0.86 \ (\mathrm{GeV}^{-2}).$$

It is also observed that most of mesons and baryons can be assigned on the Regge trajectories of straight lines [2].

A.2 Pomeron

The amplitude of the elastic scattering is related to the total cross section through the *optical theorem*,

$$\sigma_T = \frac{1}{s} \Im \mathrm{m}\{A_{ab \to ab}(s, t = 0)\}. \tag{A.6}$$

The optical theorem is shown schematically in Fig. A.3. From Eq.A.6 and Eq.A.5 we can obtain the asymptotic behavior of the total cross section for $p\bar{p}$ collision,

$$\sigma_T^{p\bar{p}} \propto s^{\alpha(0)-1} = s^{-0.45}.$$

Thus a behavior of the total cross section decreasing according to $s^{-0.45}$ is expected from the leading Regge trajectory shown in Fig. A.2.

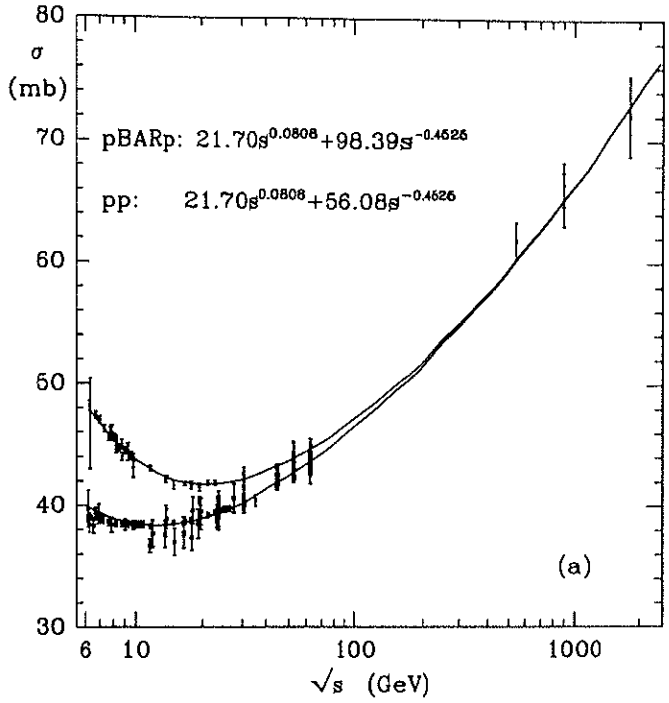

Figure A.4: Total cross-sections for p-p and p-$\bar{p}$ scattering.

Figure A.4 shows the experimental data of the total cross sections for pp and $p\bar{p}$ scattering [14]. It is evident that the total cross section is not simply falling but is slowly rising as s increases. The behavior of rising total cross section is also observed in various kind of hadron-hadron collisions. These data can be beautifully explained [14] if we accept an existence of a new Regge trajectory having the intercept of $\alpha(0)=1+\epsilon(>0)$ and it carry the quantum number of the vacuum. This new trajectory is called *pomeron trajectory* or *pomeron*. The pomeron trajectory is originally defined with the intercept of $\alpha_{I\!P}(0)=1$ to satisfy the Pomeranchuk theorem[1] and the Froissart bound[2], but the later experiments with much higher energy revealed that the situation is more complicated. The fit of the data for the total cross section and elastic

[1] A theorem which state that the total cross section against the same target become the same for particle or anti-particle in the high energy limit.

[2] It is proved that the total cross section for the two hadron scattering cannot increase faster than $(\ln s)^2$ in the limit of $s \to \infty$ in order to satisfy the unitarity of the S-matrix. This upper bound is called Froissart bound.

cross section tells us that the pomeron trajectory can be parameterized as;

$$\alpha_{I\!P}(t) = 1 + \epsilon + \alpha' t$$

where ϵ=0.0808 and α'~0.25GeV^{-2} [14]. So far now no particle has been observed on the pomeron trajectory. However, as one can see in Fig. A.4, the contribution from the pomeron trajectory become dominant in the high energy scattering.

Appendix B

CPR charge correction

The amount of charge deposition in the CPR depends on the momentum of the incident electron. The path length of the incident particle also affects the amount of charge deposition. These dependence must be corrected when one try to compare the CPR charge distributions among various samples. In the thesis, we use the *corrected CPR charge* which do not depend on neither the momentum nor the path-length. In this section, we describe how to obtain the corrected CPR charge using the track information.

As a raw CPR charge, we use a sum of outputs from three CPR-wires around an electron hit position [1]. The hit position is obtained by extrapolating the CTC track to the detector radius at the CPR layer.

The momentum and path-length dependence are studied using control samples. Conversion electrons and electrons from W decays are used for the lower and higher momentum regions, respectively.

At first we parameterize the dependence of the CPR charge on the path length by fixing the momentum range. Since the path length is related to the angle of the track, we plot the average of CPR charge as a function of $sin\theta$ in the fixed momentum ranges in Figs. B.1 and B.2. Each of these plot shows that the mean CPR charge increases as the incident angle decrease. The CPR charge increasing rate changes at $\sin\theta$=0.81. These two angle regions

[1] CDF off-line routine:get_soft_electron is used

with $\sin\theta$ above and below 0.81 correspond to the two different segments. We parameterize this angle dependence by fitting the CPR charge distribution to the two straight lines meeting at $\sin\theta = 0.81$.

$$\langle Q^{raw}_{CPR}\rangle(\theta, p^i) = \begin{cases} A_1(p^i)(\sin\theta - 1) + S(p^i) & (\sin\theta > 0.81) \\ A_2(p^i)(\sin\theta - 1) + c_2(p^i) & (\sin\theta < 0.81) \end{cases} \tag{B.1}$$

where,

$$c_2(p^i) = (0.81 - 1)(A_1(p^i) - A_2(p^i)) + S(p^i) \tag{B.2}$$

The free parameters in the above fit are $S(p^i)$, $A_1(p^i)$ and $A_2(p^i)$. We call $S(p^i)$ a scale parameter since it represents the magnitude of the CPR charge at $\sin\theta$=1. We call $A_1(p^i)$ and $A_2(p^i)$ angle parameters.

Next, we study the momentum dependence of the scale parameter $S(p^i)$. We plot $S(p^i)$ as a function of momentum in Fig. B.3. This plot is fitted to the power of the momentum;

$$S(p) = 2.8519 \times p^{0.2704} + 0.5359.$$

The first parameterizations (B.1) are divided by this and then multiplied by 10.0 to have a constant CPR charge(=10.0) at $\sin\theta$=1. New parameters are denoted with the prime(').

We then study the momentum dependence of the angle-parameters A'_1 and A'_2. We plot A'_1 and A'_2 as a function of momentum in Fig. B.4. We fit these distribution to a straight line.

$$A_1(p)' \equiv A_1(p)\frac{10}{S(p)} = -27.486 - 0.254p$$
$$A_2(p)' \equiv A_2(p)\frac{10}{S(p)} = -61.652 - 1.731p$$

Finally, the correction function which removes all momentum and angle dependence is given by;

$$Q^{cor}_{CPR} = 10.0 \times Q^{raw}_{CPR} \times F(p, \theta)$$

where,

$$F(p,\theta)^{-1} = \begin{cases} A_1(p)(sin\theta - 1) + S(p) & (sin\theta < 0.81) \\ A_2(p)(\sin\theta - 1) + (0.81 - 1)(A_1(p) - A_2(p)) + S(p) & (sin\theta > 0.81) \end{cases}$$

where,

$$\begin{aligned} S(p) &= 2.8519 \times p^{0.2704} + 0.5359 \\ A_1(p) &= \frac{S(p)}{10}(-27.486 - 0.254p) \\ A_2(p) &= \frac{S(p)}{10}(-61.652 - 1.731p). \end{aligned}$$

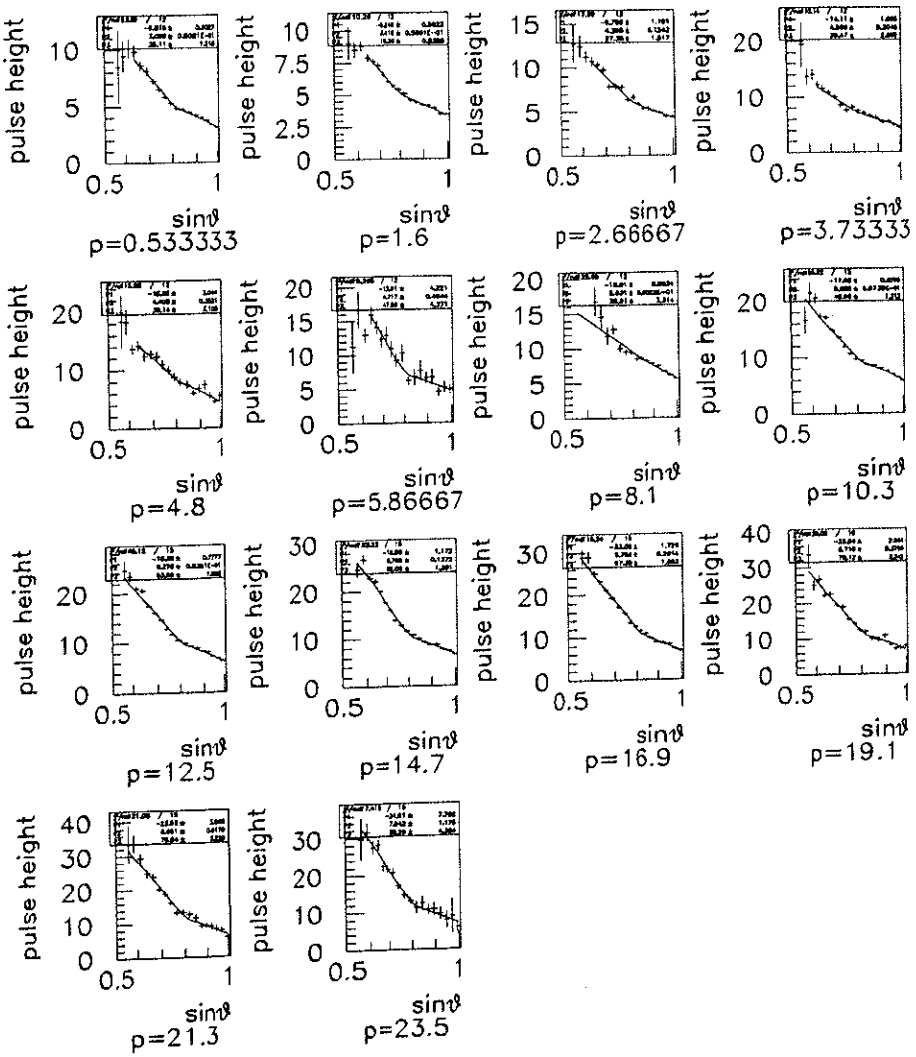

Figure B.1: The mean CPR charge versus incident angle of the electron in the fixed momentum ranges.

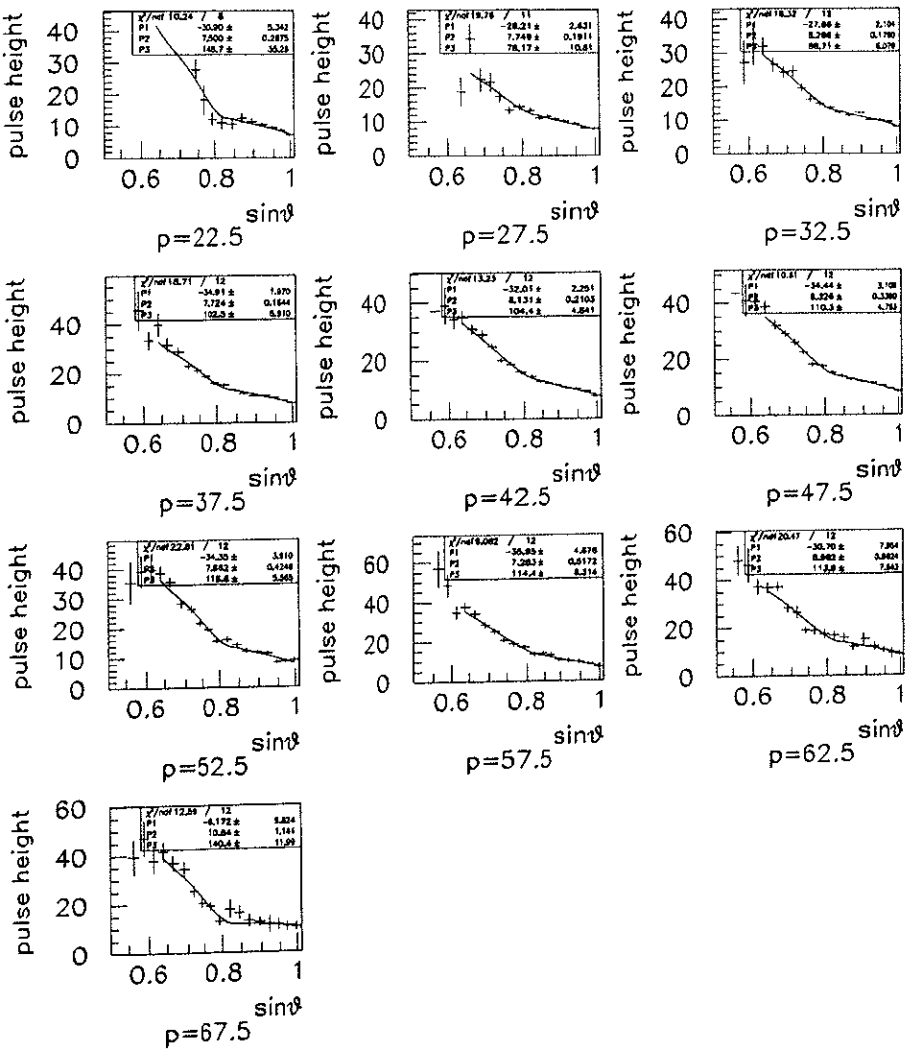

Figure B.2: The mean CPR charge versus incident angle of the electron in the fixed momentum ranges.

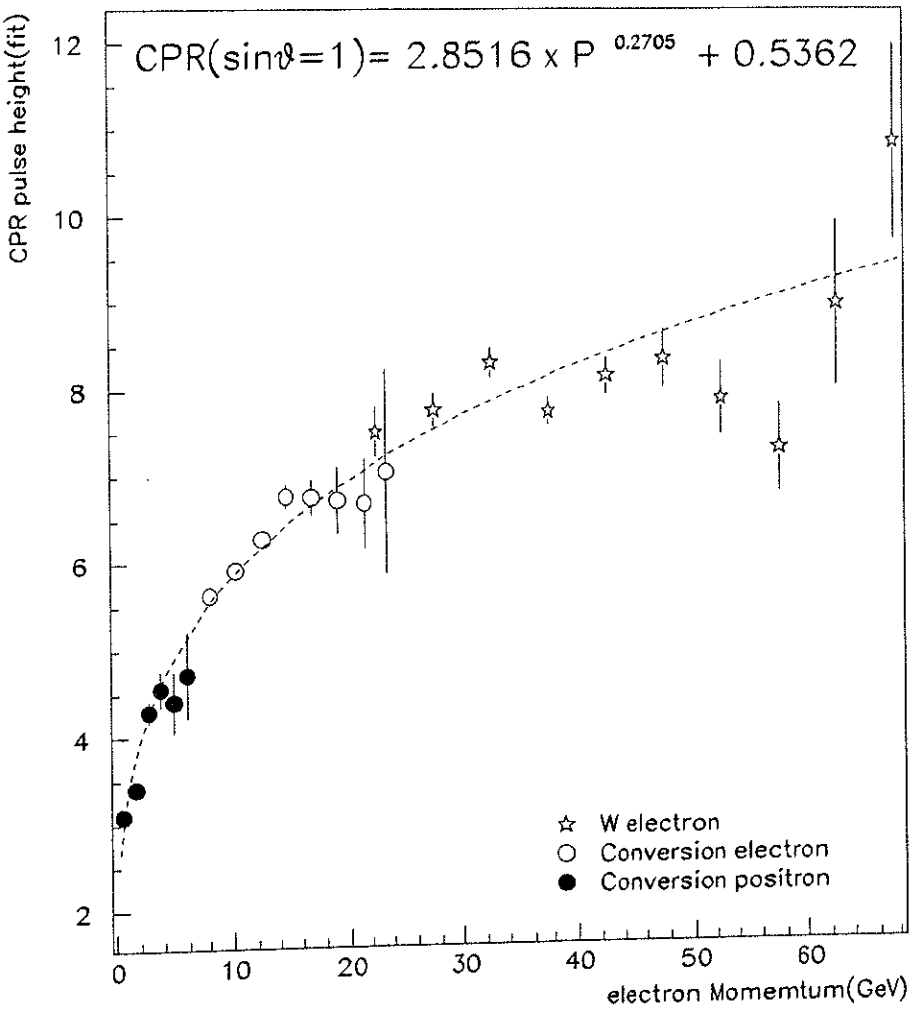

Figure B.3: The mean CPR charge versus electron momentum at $\sin\theta = 1$. The star represents for the W electron, the open circle represents for the conversion electron and the solid circle represents for the partner track of the conversion electron.

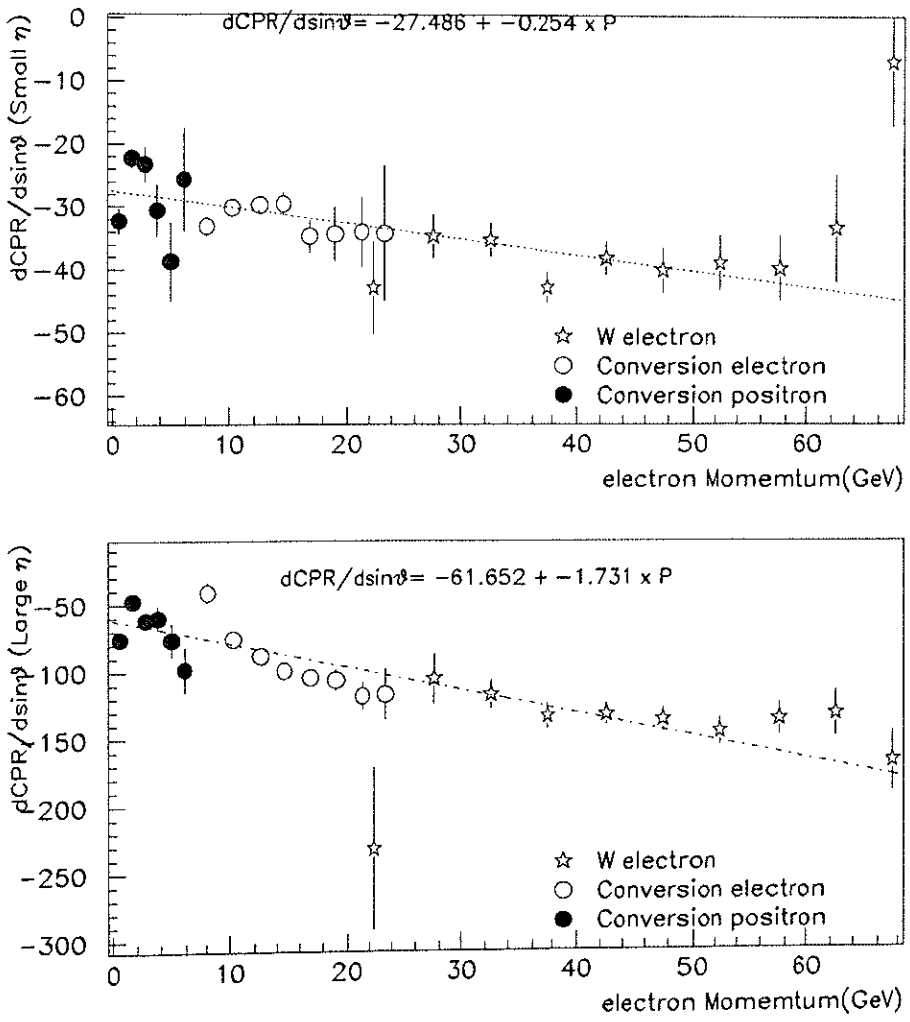

Figure B.4: $d\langle Q_{CPR}\rangle/d\sin\theta$ versus electron momentum. The star represents for the W electron, the open circle represents for the conversion electron and the solid circle represents for the partner track of the conversion electron.

Appendix C

Simulation of the forward calorimeter

We have used an established technique to simulate the detector response against the low p_T particles according to the reference [38]. The simulated energy flow in a FCAL tower is corrected by the following expression,

$$E_i^{mes} = S_i \times p^{gen} + C_i$$

where p^{gen} is a momentum of the particle in the generator-level, S_i and C_i are energy correction factors tuned in the ith η segment of the tower.

We determine the energy correction factors in order to reproduce the energies measured in the real $b\bar{b}$ sample. The selected sample of $electron + D^0$ events [39] are used as the real $b\bar{b}$ data. The D^0 mass peak of the data sets is shown in Fig. C.1. We obtained 1899 D^0 candidates during the same run as we used for the diffractive $b\bar{b}$ analysis. We then look at the exponential slopes of the energy spectra in each η segment of the forward calorimeter. Slopes of energy spectra in the D^0 mass region and the side-bands regions are shown in Fig. C.2. Since no differences are seen in the forward energy spectra between the two regions, we do not need subtract the combinatorial background from the 1899 D^0 candidates. These forward energy spectra, however, the contain contributions of energies from extra minimum bias events aside from a $b\bar{b}$ event vertex. The contribution of those pile-up events can be calculated

using the luminosity of the sample as we described in Sec. 6.1.1. We subtract the contribution of minimum bias spectra using a real data sample which is taken by the clock trigger during RUN1A period. The forward energy spectra purely coming from the $b\bar{b}$ vertex are shown in Fig. C.3.

We then look at the Monte Carlo $b\bar{b}$ sample described in the Sec. 5.1. The trajectories of all generated particles are simulated by the full detector simulation program (`CDFSIM`) and the energy flow traversing the front plane of the forward calorimeter are recorded. The real tower segmentation are used for the forward calorimeter and the energy flow in each tower are clustered as described in Sec. 3.2. The energy spectrum in each eta segment is shown in Fig. C.4. These Monte Carlo energy spectrum is much harder than the observed one. In order to match this Monte Carlo energy spectra to the observed data, we use a linear correction function as shown in the top of this section.

$$E_i^{mes} = S_i \times p^{gen} + C_i$$

The coefficients S_i and C_i are determined by comparing two spectra, the Monte Carlo and the data. Obtained energy scale factors and offset energies are shown in Fig. C.5. The error in each factors are result of the exponential fits to the energy spectra.

Matching of the forward detector simulation to the data are demonstrated in Fig. C.6 where we apply the single vertex requirement to the data so as to avoid multi-vertex effects. Since we use the energy offset around 1 GeV, our model is valid only for the energies above 1.5 GeV.

The BBC response is also simulated using the real segmentation. Only charged particles are accounted in the simulation. We do not use any energy thresholds for charged particles.

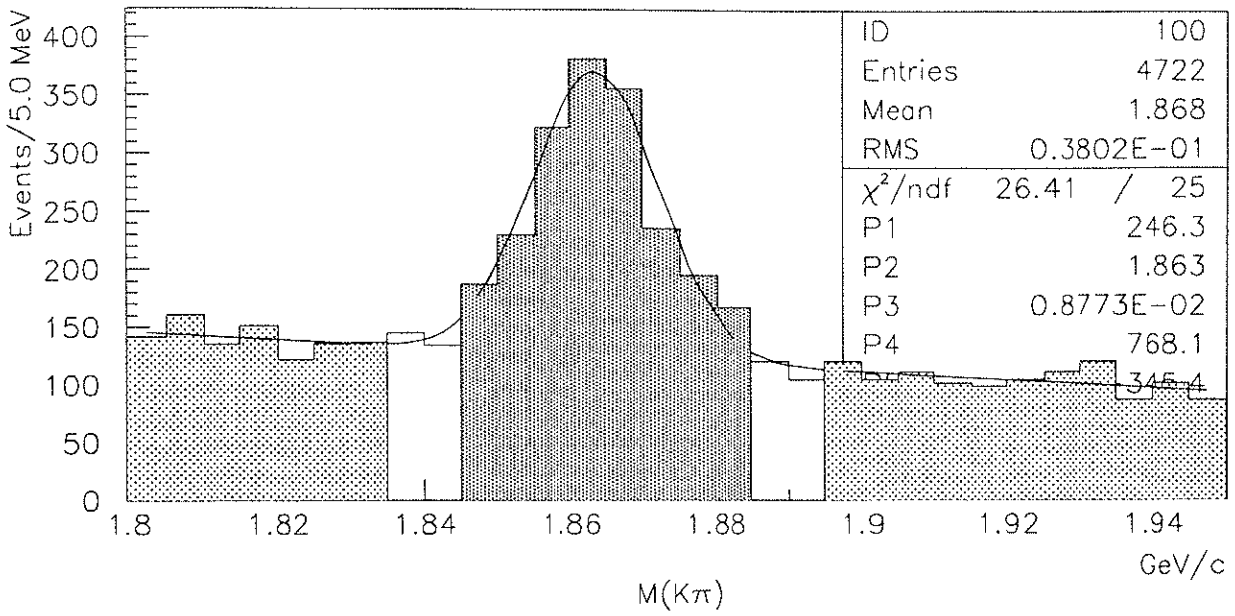

Figure C.1: The invariant mass distribution of $D^0 \to K\pi$ candidates.

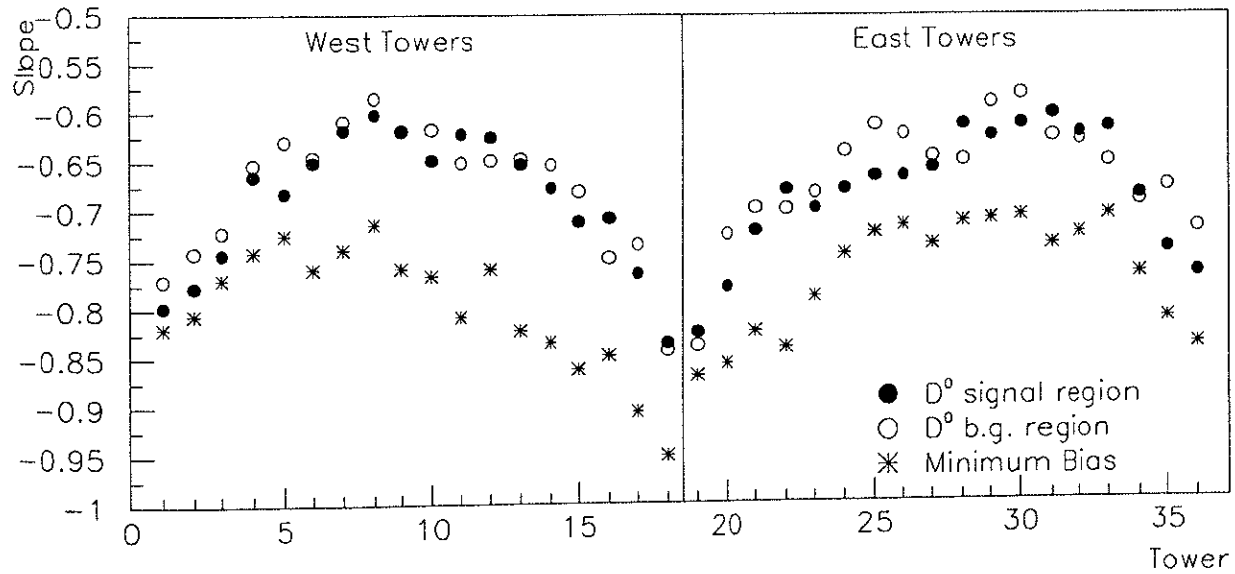

Figure C.2: The exponential slopes of the energy spectrum in each eta segments.

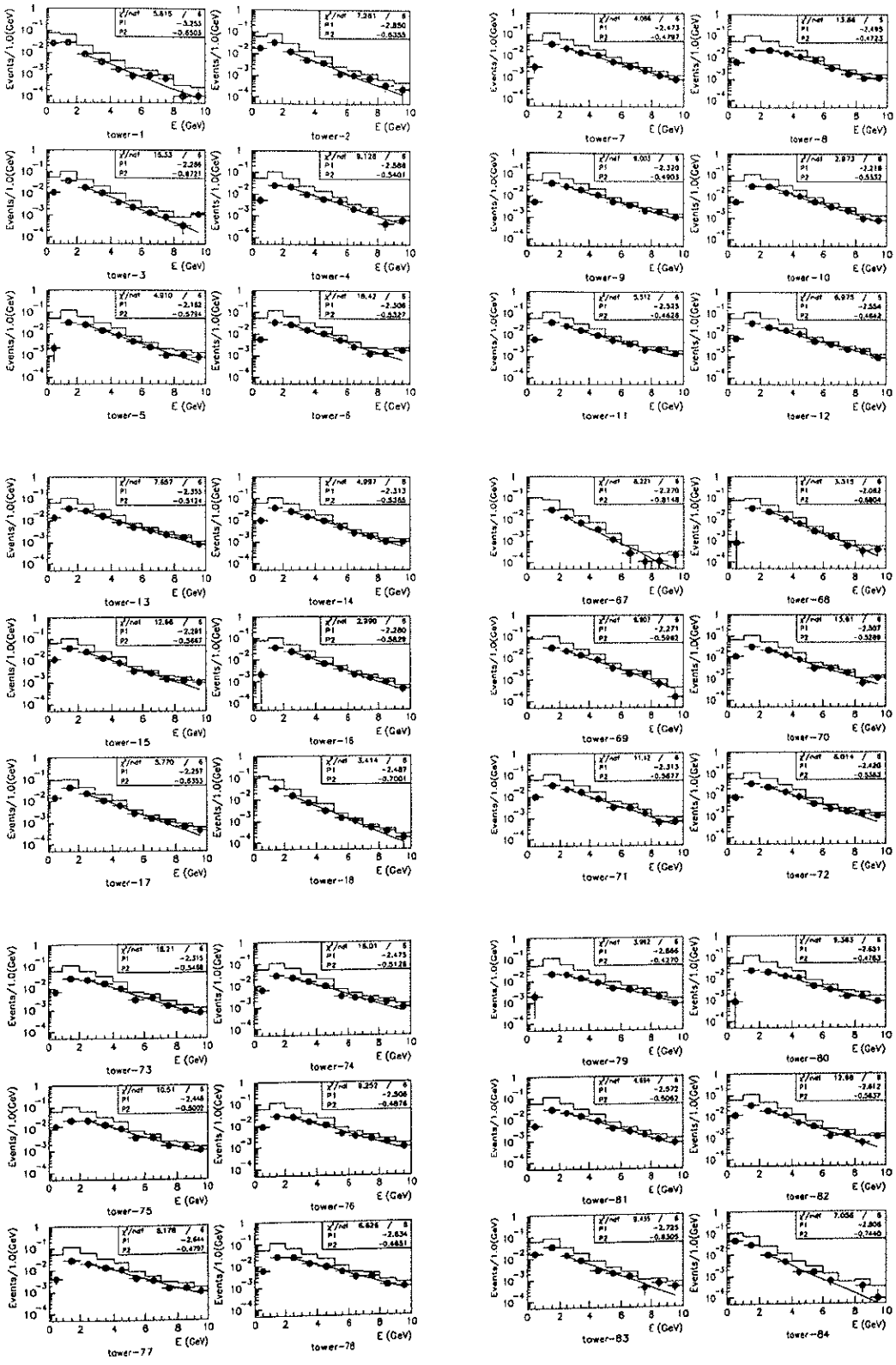

Figure C.3: The energy spectrum in each eta segments for the e+D^0 sample. The black circle shows spectra after subtracting Minimum bias contribution.

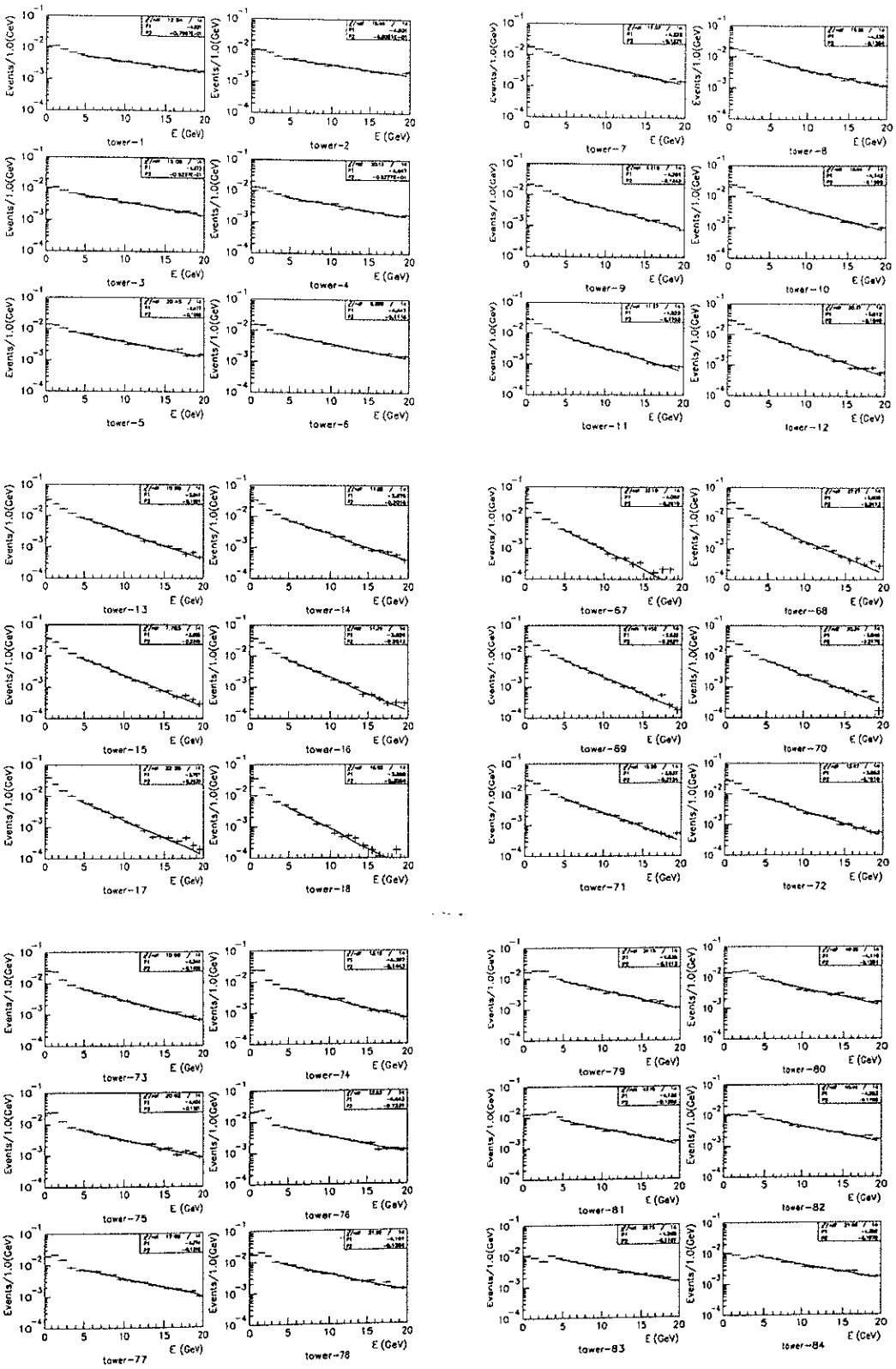

Figure C.4: The energy spectrum in each eta segments for Monte Carlo sample without any energy correction.

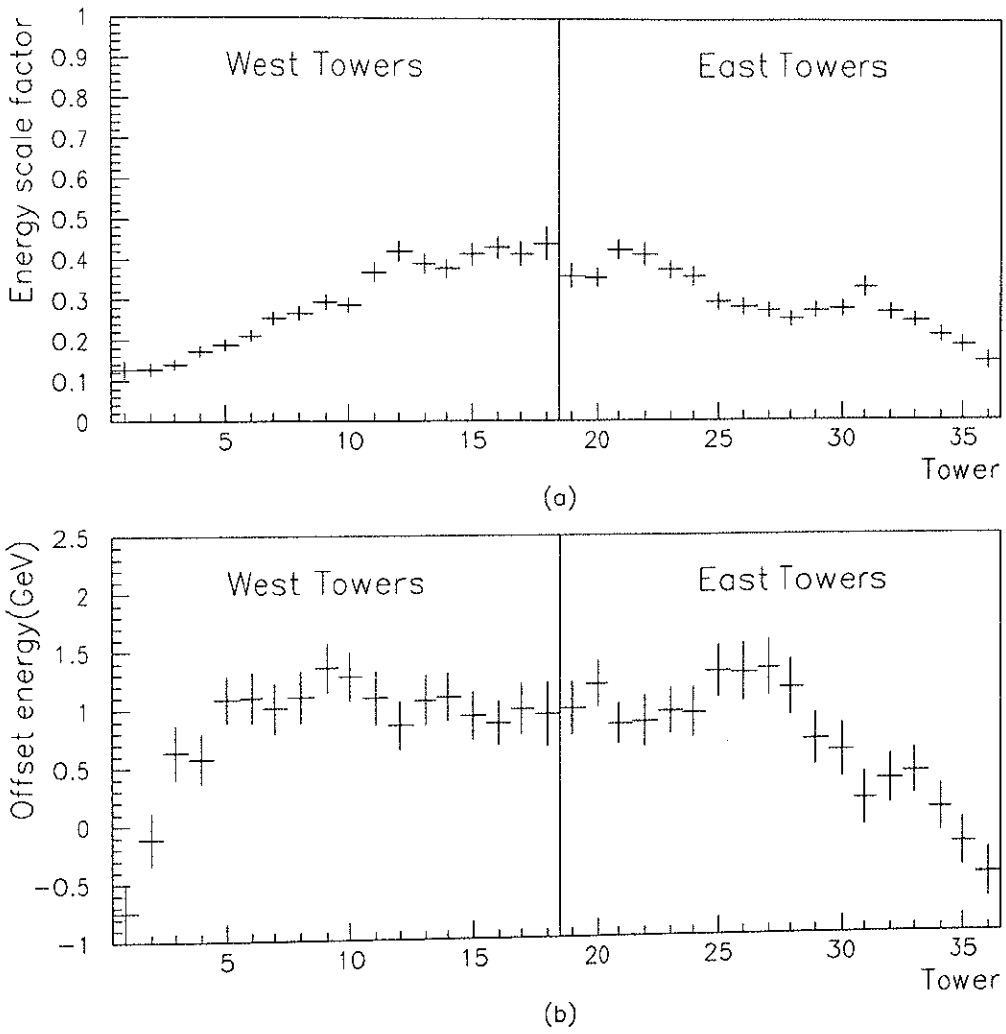

Figure C.5: The energy correction factors for Monte Carlo generated lowp_T particle. (a) the energy scale factors (b) the offset energy factors

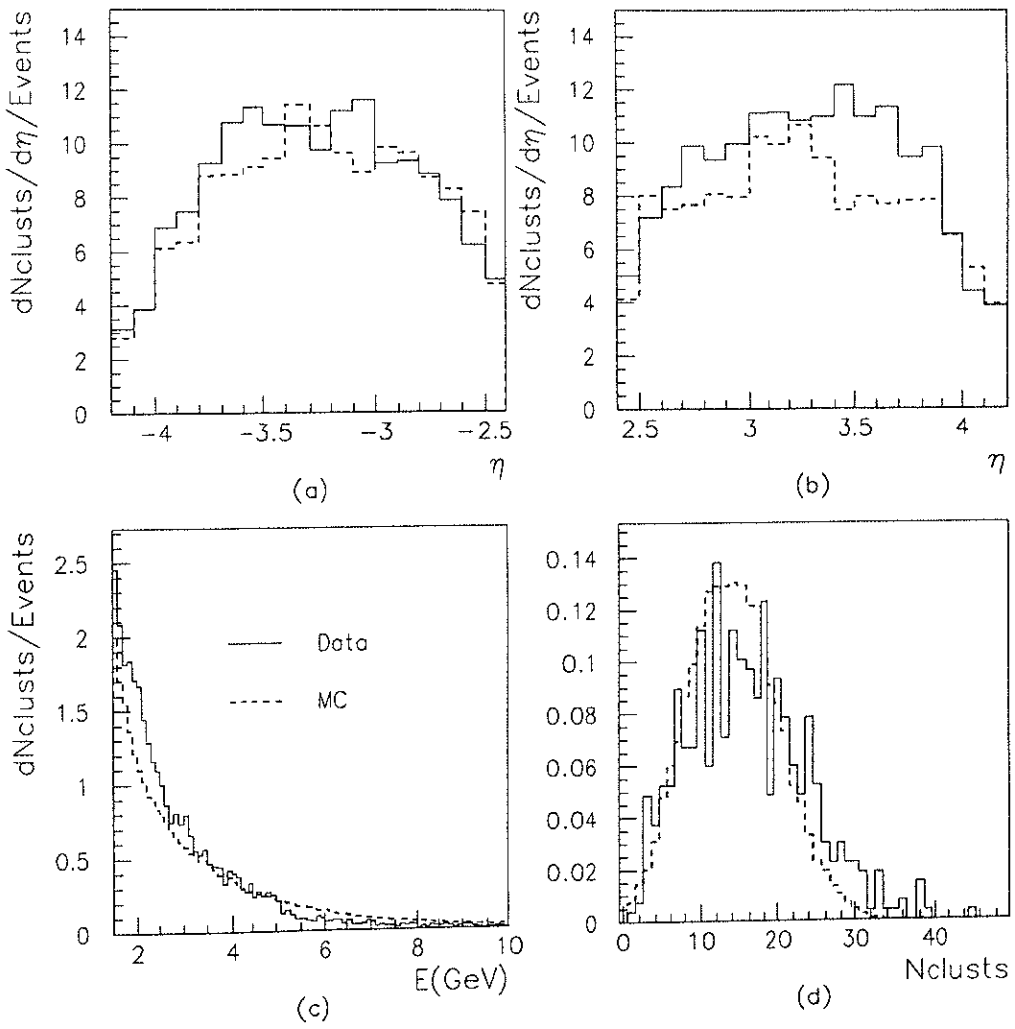

Figure C.6: Simulated response of the forward calorimeter for $b\bar{b}$ events compared to the e+D^0 sample with single vertex requirement. (a) the hit tower occupancy in the west calorimeter (b) the hit tower occupancy in the east calorimeter (c) the cluster energy spectrum (d) the number of hit clusters per events

Appendix D

Likelihood function

D.1 Likelihood function for binned fit

$$L = \frac{e^{-\mu}\mu^{N^{obs}}}{N^{obs}!} \times \frac{1}{\sqrt{2\pi}\sigma_{had}} exp\left[-\frac{1}{2}\left(\frac{n_{had} - N_{had}}{\sigma_{had}}\right)^2\right]$$
$$\times \frac{1}{\sqrt{2\pi}\sigma_{con}} exp\left[-\frac{1}{2}\left(\frac{n_{con} - N_{con}}{\sigma_{con}}\right)^2\right] \times \prod_{i=1}^{m} \frac{e^{-\mu_i}\mu_i{}^{N_i^{obs}}}{N_i^{obs}!}$$

$$\mu = n_{had} + n_{con} + n_{b\bar{b}} + n_{c\bar{c}}$$

$$\mu_i = n_{had} f_i^{had} + n_{con} f_i^{con} + n_{b\bar{b}} f_i^{b\bar{b}} + n_{c\bar{c}} f_i^{c\bar{c}}$$

parameters for fit

n_{had} = *number of hadron faking electrons*

n_{con} = *number of conversions*

$n_{b\bar{b}}$ = *number of* $b\bar{b}$ *events*

$n_{c\bar{c}}$ = *number of* $c\bar{c}$ *events*

Constants

$N^{obs} = total\ number\ of\ observed\ events$

$N_i^{obs} = number\ of\ observed\ events\ in\ the\ ith\ bin$

$N_{had} = number\ of\ hadron\ faking\ electrons\ estimated\ by\ CPR\ fit$

$\sigma_{had} = error\ of\ N_{had}$

$N_{con} = number\ of\ conversions\ estimated\ by\ conversion\ finding\ efficiency$

$\sigma_{con} = error\ of\ N_{con}$

Probability functions

$f_i^{had} = probability\ of\ a\ hadron\ having\ the\ observable\ inside\ ith\ bin$

$f_i^{con} = probability\ of\ a\ conversion\ having\ the\ observable\ inside\ ith\ bin$

$f_i^{b\bar{b}} = probability\ of\ c-electron\ having\ the\ observable\ inside\ ith\ bin$

$f_i^{c\bar{c}} = probability\ of\ b-electron\ having\ the\ observable\ inside\ ith\ bin$

D.2 Likelihood function for unbinned fit

$$
\begin{aligned}
L =& \frac{e^{-\mu}\mu^{N^{obs}}}{N^{obs}!} \times \frac{1}{\sqrt{2\pi}\sigma_{had}} exp\left[-\frac{1}{2}\left(\frac{n_{had}-N_{had}}{\sigma_{had}}\right)^2\right] \\
& \times \frac{1}{\sqrt{2\pi}\sigma_{con}} exp\left[-\frac{1}{2}\left(\frac{n_{con}-N_{con}}{\sigma_{con}}\right)^2\right] \\
& \times \prod_{j=1}^{k} \frac{n_{had}f^{had}(x_j) + n_{con}f^{con}(x_j) + n_{b\bar{b}}f^{b\bar{b}}(x_j) + n_{c\bar{c}}f^{c\bar{c}}(x_j)}{n_{had}+n_{con}+n_{b\bar{b}}+n_{c\bar{c}}} \\
\mu =& n_{had} + n_{con} + n_{b\bar{b}} + n_{c\bar{c}}
\end{aligned}
$$

parameters for fit

$n_{had} = number\ of\ hadron\ faking\ electron$

$n_{con} = number\ of\ conversions$

$n_{b\bar{b}} = number\ of\ b\bar{b}\ events$

$n_{c\bar{c}} = number\ of\ c\bar{c}\ events$

Constants

$N^{obs} = total\ number\ of\ observed\ events$

$N_{had} = number\ of\ hadron\ faking\ electrons\ estimated\ by\ CPR\ fit$

$\sigma_{had} = error\ of\ N_{had}$

$N_{con} = number\ of\ conversions\ estimated\ by\ conversion\ finding\ efficiency$

$\sigma_{con} = error\ of\ N_{con}$

Probabilityfunctions

$f^{had}(x) = probability\ of\ a\ hadron\ having\ the\ observable\ as\ x$

$f^{con}(x) = probability\ of\ a\ conversion\ having\ the\ observable\ as\ x$

$f^{b\bar{b}}(x) = probability\ of\ c-electron\ having\ the\ observable\ as\ x$

$f^{c\bar{c}}(x) = probability\ of\ b-electron\ having\ the\ observable\ as\ x$

Appendix E

The CDF Collaboration

F. Abe,[17] H. Akimoto,[39] A. Akopian,[31] M. G. Albrow,[7] A. Amadon,[5] S. R. Amendolia,[27] D. Amidei,[20] J. Antos,[33] S. Aota,[37] G. Apollinari,[31] T. Arisawa,[39] T. Asakawa,[37] W. Ashmanskas,[5] M. Atac,[7] P. Azzi-Bacchetta,[25] N. Bacchetta,[25] S. Bagdasarov,[31] M. W. Bailey,[22] P. de Barbaro,[30] A. Barbaro-Galtieri,[18] V. E. Barnes,[29] B. A. Barnett,[15] M. Barone,[9] G. Bauer,[19] T. Baumann,[11] F. Bedeschi,[27] S. Behrends,[3] S. Belforte,[27] G. Bellettini,[27] J. Bellinger,[40] D. Benjamin,[35] J. Bensinger,[3] A. Beretvas,[7] J. P. Berge,[7] J. Berryhill,[5] S. Bertolucci,[9] S. Bettelli,[27] B. Bevensee,[26] A. Bhatti,[31] K. Biery,[7] C. Bigongiari,[27] M. Binkley,[7] D. Bisello,[25] R. E. Blair,[1] C. Blocker,[3] K. Bloom,[20] S. Blusk,[30] A. Bodek,[30] W. Bokhari,[26] G. Bolla,[29] Y. Bonushkin,[4] D. Bortoletto,[29] J. Boudreau,[28] L. Breccia,[2] C. Bromberg,[21] N. Bruner,[22] R. Brunetti,[2] E. Buckley-Geer,[7] H. S. Budd,[30] K. Burkett,[11] G. Busetto,[25] A. Byon-Wagner,[7] K. L. Byrum,[1] M. Campbell,[20] A. Caner,[27] W. Carithers,[18] D. Carlsmith,[40] J. Cassada,[30] A. Castro,[25] D. Cauz,[36] A. Cerri,[27] P. S. Chang,[33] P. T. Chang,[33] H. Y. Chao,[33] J. Chapman,[20] M. -T. Cheng,[33] M. Chertok,[34] G. Chiarelli,[27] C. N. Chiou,[33] F. Chlebana,[7] L. Christofek,[13] R. Cropp,[14] M. L. Chu,[33] S. Cihangir,[7] A. G. Clark,[10] M. Cobal,[27] E. Cocca,[27] M. Contreras,[5] J. Conway,[32] J. Cooper,[7] M. Cordelli,[9] D. Costanzo,[27] C. Couyoumtzelis,[10] D. Cronin-Hennessy,[6] R. Culbertson,[5]

D. Dagenhart,[38] T. Daniels,[19] F. DeJongh,[7] S. Dell'Agnello,[9] M. Dell'Orso,[27] R. Demina,[7] L. Demortier,[31] M. Deninno,[2] P. F. Derwent,[7] T. Devlin,[32] J. R. Dittmann,[6] S. Donati,[27] J. Done,[34] T. Dorigo,[25] N. Eddy,[13] K. Einsweiler,[18] J. E. Elias,[7] R. Ely,[18] E. Engels, Jr.,[28] W. Erdmann,[7] D. Errede,[13] S. Errede,[13] Q. Fan,[30] R. G. Feild,[41] Z. Feng,[15] C. Ferretti,[27] I. Fiori,[2] B. Flaugher,[7] G. W. Foster,[7] M. Franklin,[11] J. Freeman,[7] J. Friedman,[19] H. Frisch,[5] Y. Fukui,[17] S. Gadomski,[14] S. Galeotti,[27] M. Gallinaro,[26] O. Ganel,[35] M. Garcia-Sciveres,[18] A. F. Garfinkel,[29] C. Gay,[41] S. Geer,[7] D. W. Gerdes,[20] P. Giannetti,[27] N. Giokaris,[31] P. Giromini,[9] G. Giusti,[27] M. Gold,[22] A. Gordon,[11] A. T. Goshaw,[6] Y. Gotra,[28] K. Goulianos,[31] H. Grassmann,[36] C. Green,[29] L. Groer,[32] C. Grosso-Pilcher,[5] G. Guillian,[20] J. Guimaraes da Costa,[15] R. S. Guo,[33] C. Haber,[18] E. Hafen,[19] S. R. Hahn,[7] R. Hamilton,[11] T. Handa,[12] R. Handler,[40] W. Hao,[35] F. Happacher,[9] K. Hara,[37] A. D. Hardman,[29] R. M. Harris,[7] F. Hartmann,[16] J. Hauser,[4] E. Hayashi,[37] J. Heinrich,[26] A. Heiss,[16] B. Hinrichsen,[14] K. D. Hoffman,[29] C. Holck,[26] R. Hollebeek,[26] L. Holloway,[13] Z. Huang,[20] B. T. Huffman,[28] R. Hughes,[23] J. Huston,[21] J. Huth,[11] H. Ikeda,[37] M. Incagli,[27] J. Incandela,[7] G. Introzzi,[27] J. Iwai,[39] Y. Iwata,[12] E. James,[20] H. Jensen,[7] U. Joshi,[7] E. Kajfasz,[25] H. Kambara,[10] T. Kamon,[34] T. Kaneko,[37] K. Karr,[38] H. Kasha,[41] Y. Kato,[24] T. A. Keaffaber,[29] K. Kelley,[19] R. D. Kennedy,[7] R. Kephart,[7] D. Kestenbaum,[11] D. Khazins,[6] T. Kikuchi,[37] M. Kirk,[3] B. J. Kim,[27] H. S. Kim,[14] S. H. Kim,[37] Y. K. Kim,[18] L. Kirsch,[3] S. Klimenko,[8] D. Knoblauch,[16] P. Koehn,[23] A. Köngeter,[16] K. Kondo,[37] J. Konigsberg,[8] K. Kordas,[14] A. Korytov,[8] E. Kovacs,[1] W. Kowald,[6] J. Kroll,[26] M. Kruse,[30] S. E. Kuhlmann,[1] E. Kuns,[32] K. Kurino,[12] T. Kuwabara,[37] A. T. Laasanen,[29] S. Lami,[27] S. Lammel,[7] J. I. Lamoureux,[3] M. Lancaster,[18] M. Lanzoni,[27] G. Latino,[27] T. LeCompte,[1] S. Leone,[27] J. D. Lewis,[7] M. Lindgren,[4] T. M. Liss,[13] J. B. Liu,[30] Y. C. Liu,[33]

N. Lockyer,[26] O. Long,[26] M. Loreti,[25] D. Lucchesi,[27] P. Lukens,[7] S. Lusin,[40] J. Lys,[18] K. Maeshima,[7] P. Maksimovic,[11] M. Mangano,[27] M. Mariotti,[25] J. P. Marriner,[7] G. Martignon,[25] A. Martin,[41] J. A. J. Matthews,[22] P. Mazzanti,[2] K. McFarland,[30] P. McIntyre,[34] P. Melese,[31] M. Menguzzato,[25] A. Menzione,[27] E. Meschi,[27] S. Metzler,[26] C. Miao,[20] T. Miao,[7] G. Michail,[11] R. Miller,[21] H. Minato,[37] S. Miscetti,[9] M. Mishina,[17] S. Miyashita,[37] N. Moggi,[27] E. Moore,[22] Y. Morita,[17] A. Mukherjee,[7] T. Muller,[16] A. Munar,[27] P. Murat,[27] S. Murgia,[21] M. Musy,[36] H. Nakada,[37] T. Nakaya,[5] I. Nakano,[12] C. Nelson,[7] D. Neuberger,[16] C. Newman-Holmes,[7] C.-Y. P. Ngan,[19] H. Niu,[3] L. Nodulman,[1] A. Nomerotski,[8] S. H. Oh,[6] T. Ohmoto,[12] T. Ohsugi,[12] R. Oishi,[37] M. Okabe,[37] T. Okusawa,[24] J. Olsen,[40] C. Pagliarone,[27] R. Paoletti,[27] V. Papadimitriou,[35] S. P. Pappas,[41] N. Parashar,[27] A. Parri,[9] D. Partos,[3] J. Patrick,[7] G. Pauletta,[36] M. Paulini,[18] A. Perazzo,[27] L. Pescara,[25] M. D. Peters,[18] T. J. Phillips,[6] G. Piacentino,[27] M. Pillai,[30] K. T. Pitts,[7] R. Plunkett,[7] A. Pompos,[29] L. Pondrom,[40] J. Proudfoot,[1] F. Ptohos,[11] G. Punzi,[27] K. Ragan,[14] D. Reher,[18] M. Reischl,[16] A. Ribon,[25] F. Rimondi,[2] L. Ristori,[27] W. J. Robertson,[6] A. Robinson,[14] T. Rodrigo,[27] S. Rolli,[38] L. Rosenson,[19] R. Roser,[13] T. Saab,[14] W. K. Sakumoto,[30] D. Saltzberg,[4] A. Sansoni,[9] L. Santi,[36] H. Sato,[37] P. Schlabach,[7] E. E. Schmidt,[7] M. P. Schmidt,[41] A. Scott,[4] A. Scribano,[27] S. Segler,[7] S. Seidel,[22] Y. Seiya,[37] F. Semeria,[2] T. Shah,[19] M. D. Shapiro,[18] N. M. Shaw,[29] P. F. Shepard,[28] T. Shibayama,[37] M. Shimojima,[37] M. Shochet,[5] J. Siegrist,[18] A. Sill,[35] P. Sinervo,[14] P. Singh,[13] K. Sliwa,[38] C. Smith,[15] F. D. Snider,[15] J. Spalding,[7] T. Speer,[10] P. Sphicas,[19] F. Spinella,[27] M. Spiropulu,[11] L. Spiegel,[7] L. Stanco,[25] J. Steele,[40] A. Stefanini,[27] R. Ströhmer,[7a] J. Strologas,[13] F. Strumia, [10] D. Stuart,[7] K. Sumorok,[19] J. Suzuki,[37] T. Suzuki,[37] T. Takahashi,[24] T. Takano,[24] R. Takashima,[12] K. Takikawa,[37] M. Tanaka,[37]

B. Tannenbaum,[4] F. Tartarelli,[27] W. Taylor,[14] M. Tecchio,[20] P. K. Teng,[33] Y. Teramoto,[24] K. Terashi,[37] S. Tether,[19] D. Theriot,[7] T. L. Thomas,[22] R. Thurman-Keup,[1] M. Timko,[38] P. Tipton,[30] A. Titov,[31] S. Tkaczyk,[7] D. Toback,[5] K. Tollefson,[30] A. Tollestrup,[7] H. Toyoda,[24] W. Trischuk,[14] J. F. de Troconiz,[11] S. Truitt,[20] J. Tseng,[19] N. Turini,[27] T. Uchida,[37] F. Ukegawa,[26] J. Valls,[32] S. C. van den Brink,[15] S. Vejcik, III,[20] G. Velev,[27] I. Volobouev,[18] R. Vidal,[7] R. Vilar,[7a] D. Vucinic,[19] R. G. Wagner,[1] R. L. Wagner,[7] J. Wahl,[5] N. B. Wallace,[27] A. M. Walsh,[32] C. Wang,[6] C. H. Wang,[33] M. J. Wang,[33] A. Warburton,[14] T. Watanabe,[37] T. Watts,[32] R. Webb,[34] C. Wei,[6] H. Wenzel,[16] W. C. Wester, III,[7] A. B. Wicklund,[1] E. Wicklund,[7] R. Wilkinson,[26] H. H. Williams,[26] P. Wilson,[7] B. L. Winer,[23] D. Winn,[20] D. Wolinski,[20] J. Wolinski,[21] S. Worm,[22] X. Wu,[10] J. Wyss,[27] A. Yagil,[7] W. Yao,[18] K. Yasuoka,[37] G. P. Yeh,[7] P. Yeh,[33] J. Yoh,[7] C. Yosef,[21] T. Yoshida,[24] I. Yu,[7] A. Zanetti,[36] F. Zetti,[27] and S. Zucchelli[2]

(CDF Collaboration)

[1] *Argonne National Laboratory, Argonne, Illinois 60439*

[2] *Istituto Nazionale di Fisica Nucleare, University of Bologna, I-40127 Bologna, Italy*

[3] *Brandeis University, Waltham, Massachusetts 02254*

[4] *University of California at Los Angeles, Los Angeles, California 90024*

[5] *University of Chicago, Chicago, Illinois 60637*

[6] *Duke University, Durham, North Carolina 27708*

[7] *Fermi National Accelerator Laboratory, Batavia, Illinois 60510*

[8] *University of Florida, Gainesville, Florida 32611*

[9] *Laboratori Nazionali di Frascati, Istituto Nazionale di Fisica Nucleare, I-00044 Frascati, Italy*

[10] *University of Geneva, CH-1211 Geneva 4, Switzerland*

[11] *Harvard University, Cambridge, Massachusetts 02138*

[12] *Hiroshima University, Higashi-Hiroshima 724, Japan*

[13] *University of Illinois, Urbana, Illinois 61801*

[14] *Institute of Particle Physics, McGill University, Montreal H3A 2T8, and University of Toronto, Toronto M5S 1A7, Canada*

[15] *The Johns Hopkins University, Baltimore, Maryland 21218*

[16] *Institut für Experimentelle Kernphysik, Universität Karlsruhe, 76128 Karlsruhe, Germany*

[17] *National Laboratory for High Energy Physics (KEK), Tsukuba, Ibaraki 305, Japan*

[18] *Ernest Orlando Lawrence Berkeley National Laboratory, Berkeley, California 94720*

[19] *Massachusetts Institute of Technology, Cambridge, Massachusetts 02139*

[20] *University of Michigan, Ann Arbor, Michigan 48109*

[21] *Michigan State University, East Lansing, Michigan 48824*

[22] *University of New Mexico, Albuquerque, New Mexico 87131*

[23] *The Ohio State University, Columbus, Ohio 43210*

[24] *Osaka City University, Osaka 588, Japan*

[25] *Universita di Padova, Istituto Nazionale di Fisica Nucleare, Sezione di Padova, I-35131 Padova, Italy*

[26] *University of Pennsylvania, Philadelphia, Pennsylvania 19104*

[27] *Istituto Nazionale di Fisica Nucleare, University and Scuola Normale Superiore of Pisa, I-56100 Pisa, Italy*

[28] *University of Pittsburgh, Pittsburgh, Pennsylvania 15260*

[29] *Purdue University, West Lafayette, Indiana 47907*

[30] *University of Rochester, Rochester, New York 14627*

[31] *Rockefeller University, New York, New York 10021*

[32] *Rutgers University, Piscataway, New Jersey 08855*

[33] *Academia Sinica, Taipei, Taiwan 11530, Republic of China*

[34] *Texas A&M University, College Station, Texas 77843*

[35] *Texas Tech University, Lubbock, Texas 79409*

[36] *Istituto Nazionale di Fisica Nucleare, University of Trieste/ Udine, Italy*

[37] *University of Tsukuba, Tsukuba, Ibaraki 305, Japan*

[38] *Tufts University, Medford, Massachusetts 02155*

[39] *Waseda University, Tokyo 169, Japan*

[40] *University of Wisconsin, Madison, Wisconsin 53706*

[41] *Yale University, New Haven, Connecticut 06520*